JACS
JOURNAL OF THE AMERICAN CHEMICAL SOCIETY
Article
pubs.acs.org/JACS

Locating Protonated Amines in Clathrates

Terrence M. Chang, Richard J. Cooper, and Evan R. Williams*

Department of Chemistry, University of California, Berkeley, California 94720-1460, United States

Supporting Information

ABSTRACT: The structures and inherent stabilities of hydrated, protonated ammonia, select protonated primary, secondary, and tertiary amines as well as tetramethylammonium with 19−21 water molecules were investigated using infrared photodissociation (IRPD) spectroscopy and blackbody infrared radiative dissociation (BIRD) at 133 K. Magic number clusters (MNCs) with 20 water molecules were observed for all ions except tetramethylammonium, and the BIRD results indicate that these clusters have stable structures, which are relatively unaffected by addition of one water molecule but are disrupted in clusters with one less water molecule. IRPD spectra in the water free O−H stretch region are consistent with clathrate structures for the MNCs with 20 water molecules, whereas nonclathrate structures are indicated for tetramethylammonium as well as ions at the other cluster sizes. The locations of protonated ammonia and the protonated primary amines either in the interior or at the surface of a clathrate were determined by comparing IRPD spectra of these ions to those of reference ions; Rb^+ and protonated *tert*-butylammonia with 20 water molecules were used as references for an ion in the interior and at the surface of a clathrate, respectively. These results indicate that protonated ammonia is in the interior of the clathrate, whereas protonated methyl- and *n*-heptylamine are at the surface. Calculations suggest that the number of hydrogen bonds in these clusters does not directly correlate with structural stability, indicating that both the number and orientation of the hydrogen bonds are important. These experimental results should serve as benchmarks for computational studies aimed at elucidating ion effects on the hydrogen-bonding network of water molecules and the surface activity of ions.

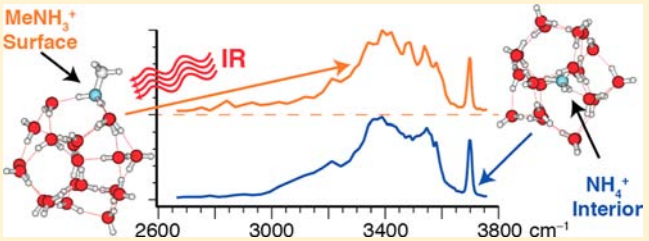

INTRODUCTION

Interfaces are important in many different chemical and biochemical processes, ranging from drug delivery,[1−3] protein folding,[4,5] and assembly of macromolecular complexes[6,7] to reactions at aerosol surfaces relevant to atmospheric chemistry.[8−11] Hydrogen-bonding networks of water are affected by interfaces, such as those between water and air or water and proteins. Hydrogen-bonding networks are also influenced by ions,[12−18] and ion−water interactions play an important role in the Hofmeister phenomena[19−21] as well as the surface activity of ions.[22] The latter can significantly affect reaction rates at surfaces. For example, formation of Br_2 from the surface active ion, Br^-, occurs up to 4 orders of magnitude faster at the surface of an aerosol than it does in solution.[8] The surface activity of an ion depends on several factors, including the ion's polarizability[23,24] and charge state.[25] Investigating how ions interact with solvating water molecules can lead to a better understanding of both surface activity and the extent to which ions can influence the hydrogen-bonding network of water.

Detailed information about ion−water interactions can be obtained from studies of gas-phase hydrated ions, where clusters can be size selected and subsequently characterized by a wide variety of structural methods. Inner shell coordination numbers,[14,26−30] sequential water molecule binding energies,[31−39] and the effect of hydration on molecular structure[40−43] have been investigated. IR spectroscopy is a powerful technique for obtaining structural information and has been used to investigate the effect of water on zwitterion stability,[40] molecular folding,[43,44] and ion effects on the hydrogen-bonding network of water molecules.[14−18,26−30,45−49]

Some hydrated ions in cluster distributions can have enhanced abundances compared to adjacent sized clusters.[47−59] These ions, often referred to as magic number clusters (MNCs), often indicate especially stable structures. MNCs with 20 water molecules have been reported for a variety of ions, including H_3O^+, NH_4^+, K^+, Rb^+, and Cs^+, and have been attributed to the formation of cage-like clathrate structures.[46−49,51,59−79] Clathrates are common in nature where they have been implicated in global climate change[80] and blocking of oil pipelines.[81] Clathrates also have potential practical applications, such as sequestration of greenhouse gases[82−84] and are a significant reservoir of natural gas.[85−87]

One of the most widely investigated MNCs is $H_3O^+ \cdot (H_2O)_{20}$, for which a clathrate structure has been deduced from computational chemistry,[59,68−75] IR spectroscopy,[46,47] and ion molecule reactivity.[79] The IR spectrum of this ion has a single peak in the free O−H stretch region corresponding to water molecules that accept two hydrogen bonds (HBs) and donate one HB to adjacent water molecules (acceptor−acceptor−donor, or AAD, water molecules), which is characteristic of a clathrate structure.[46,47] However, the location of the proton,

Received: July 19, 2013
Published: September 5, 2013

   dx.doi.org/10.1021/ja407414d | J. Am. Chem. Soc. 2013, 135, 14821−14830

whether in the interior or at the surface of a clathrate structure, could not be determined from these experiments alone. Early computational studies indicated that the proton is located in the interior,[59,68−70] but more recent calculations suggest that the proton is at the surface.[71−75] Both experimental[48] and computational[64−67] results indicate that larger alkali metal ions fit into a clathrate cage when hydrated by 20 water molecules, but Na^+ does not. Results for $Li^+\cdot(H_2O)_{20}$ suggest that a fraction of the ion population adopts clathrate structures, indicating that these structures depend both on the ion size and how the ions affect the hydrogen-bonding network of the water molecules.[48,88]

$NH_4^+\cdot(H_2O)_{20}$ is also a MNC, and the IR spectrum of this ion reported by Diken et al. has the characteristic AAD free O−H stretch indicative of clathrate structure.[49] As was the case for $H_3O^+\cdot(H_2O)_{20}$, the location of the ion could not be determined solely from the spectroscopy data. Computed enthalpies of formation for various structures suggest that it is more favorable for the ion to be located at the surface than in the interior by ∼40 kJ mol^{-1},[49] consistent with a previous computational study.[76] However, formation enthalpies from recent computational studies indicate that structures with NH_4^+ in the interior are more favorable by ∼10 kJ mol^{-1}.[77,78] Computations suggest that the charge is localized on the ammonium moiety (vs neutral ammonia and a hydronium ion),[76] whereas an excess proton is highly mobile in a pure water network,[89−92] even at the surface of $H_3O^+\cdot(H_2O)_{20}$ clathrates.[61] This may affect the preferred location of an ion in a clathrate.

Here, the locations of the ions either at the surface or in the interior of a clathrate structure when hydrated by 20 water molecules were determined by comparing spectra of $NH_4^+\cdot(H_2O)_{20}$ and $RNH_3^+\cdot(H_2O)_{20}$ (R = methyl- and *n*-heptyl-alkyl groups) to spectra of reference ions for which the location of the ion can be confidently assigned. From these comparisons, we conclude that $NH_4^+\cdot(H_2O)_{20}$ is in the interior of a clathrate, whereas primary alkylamines are at the surface of a clathrate. This is the first experimental evidence for the location of these ions either in the interior or at the surface of clathrates. These results provide insight into clathrate structures and how guest ions affect the hydrogen-bonding network of water molecules in these structures.

EXPERIMENTAL SECTION

Mass Spectrometry and Spectroscopy. All experimental data were obtained using a 7.0 T Fourier transform ion cyclotron resonance (FT/ICR) mass spectrometer. This instrument is based on a 2.75 T FT/ICR instrument described elsewhere[93] but with a higher field strength magnet and modified vacuum chamber. The protonated forms of the following molecules: NH_3, methyl-, *n*-heptyl-, *tert*-butyl-, dimethyl-, and trimethylammonia (MonMA$^+$, nHA$^+$, tBA$^+$, DiMA$^+$, and TriMA$^+$, respectively) as well as tetramethylammonium ions (TetMA$^+$) (Figure 1) were formed by nanoelectrospray (nanoESI) from 3−5 mM solutions using water purified by a Milli-Q purification system (Millipore, Billerica, MA, U.S.A.). All chemicals were obtained from Sigma-Aldrich (St. Louis, MO, U.S.A.). Borosilicate capillaries that are pulled to an inner tip diameter of ∼1 μm and filled with the analyte-containing aqueous solution are used to form ions by nanoESI. A platinum filament in contact with the sample solution is held at a potential of 700−900 V relative to the heated metal capillary of the nanoESI interface. Ions are guided by electrostatic lenses through five stages of differential pumping into the ion cell. The temperature of the ion cell is controlled by a surrounding copper jacket that is cooled by a regulated flow of liquid nitrogen.[94] Prior to experiments, the cell is cooled to 133 K for a minimum of 8 h. A pulse of dry nitrogen gas (∼10^{-6} Torr) is introduced into the vacuum chamber containing the ion cell for ∼5 s to improve ion trapping and thermalization. After a ∼7 s pumpdown delay following the introduction of pulse gas, the pressure inside the cell is <10^{-8} Torr. Precursor ions are subsequently mass selected using a stored waveform inverse Fourier transform.

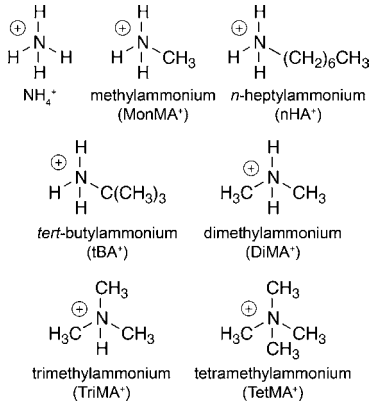

Figure 1. Structures and abbreviations for ammonium and alkylammonium ions investigated.

Blackbody infrared radiative dissociation (BIRD) rate constants are obtained from the precursor and product ion abundances as a result of dissociation from absorption of blackbody photons from the ion cell and cell jacket for times between 0.5 and 5.0 s. Infrared photodissociation (IRPD) spectra are measured by irradiating the mass selected precursor ions with tunable IR photons generated by an OPO/OPA system (LaserVision, Bellevue, WA, U.S.A.) that is pumped by the 1064 nm fundamental of a Nd:YAG laser (Continuum Surelight I-10, Santa Clara, CA, U.S.A.) pulsed at a 10 Hz repetition rate. The IRPD rate constants are corrected for frequency-dependent variations in laser power as well as BIRD.[95] Irradiation times were chosen so that substantial, but not complete, dissociation of the precursor occurred. The relative intensities of bands in the free O−H region (∼3640−3780 cm^{-1}) were determined from the integrated areas of Gaussian peaks fitted to the experimental data using Igor v 6.00 (Wavemetrics, Portland, OR, U.S.A.).

Computational Chemistry. Conformational searches for tBA$^+$, DiMA$^+$, TriMA$^+$, and TetMA$^+$ with 20 water molecules attached were performed with Macromodel 9.1 (Schrödinger, Inc., Portland, OR, U.S.A.) using MMFFs or OPLS2005 force fields. The 10 lowest-energy structures from each conformational search were then optimized at the B3LYP/6-31+G** level of theory using Q-Chem 4.0 (Q-Chem, Inc., Pittsburgh, PA, U.S.A.).[96] Additional structures based on those reported for $H_3O^+\cdot(H_2O)_{20}$ were also optimized at the same level of theory.[47] Relative Gibbs free energies at 133 K were calculated from zero-point energies, enthalpy and entropy corrections using unscaled B3LYP/6-31+G** harmonic oscillator vibrational frequencies.

RESULTS AND DISCUSSION

Magic Number Clusters for Hydrated Ammonium Ions. A broad distribution of hydrated ions: NH_4^+, MonMA$^+$, nHA$^+$, tBA$^+$, DiMA$^+$, TriMA$^+$, and TetMA$^+$ can be readily produced by nanoESI from aqueous solutions, and these distributions can be shifted to smaller or larger average sizes by varying experimental conditions. The relative abundances of these different hydrated ions as a function of cluster size, measured with the same experimental conditions, are shown in Figure 2. The abundances of several clusters are higher than those of adjacent clusters. Most notably, the abundances of clusters with 20 water molecules are significantly higher than those of n = 19 or 21 for all ions except TetMA$^+$ and only marginally so for DiMA$^+$. These MNCs at n = 20 are consistent with previous studies on hydrated ammonium, alkylammonium, and NH_4^+·pyridine ions,[49,53−55,58] with the exception of

dx.doi.org/10.1021/ja407414d | J. Am. Chem. Soc. 2013, 135, 14821−14830

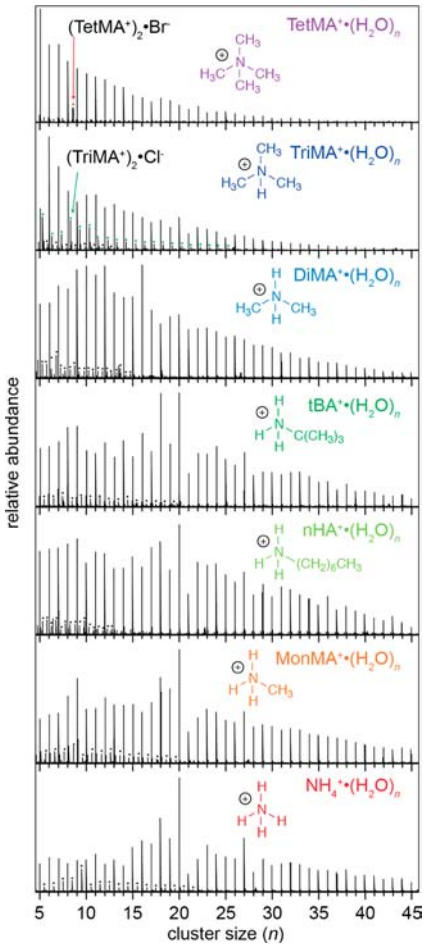

Figure 2. Abundances of hydrated ammonium ions formed by nanoESI as a function of cluster size (n). Chemical interferences are labeled with red or green squares corresponding to $(TetMA^+)_2{\cdot}Br^-$ and $(TriMA^+)_2{\cdot}Cl^-$, respectively. Second harmonics are labeled with black circles.

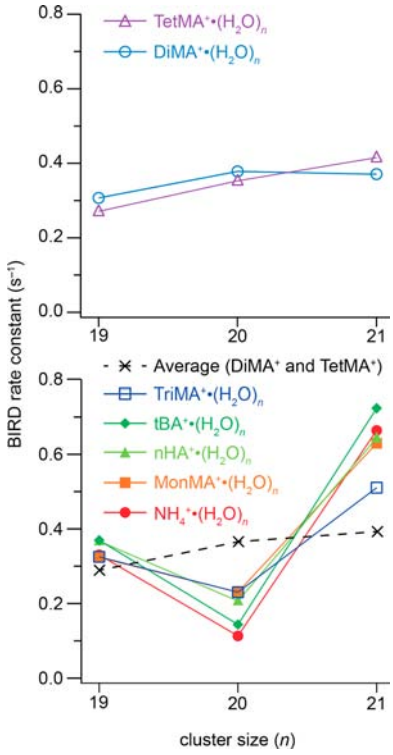

Figure 3. BIRD rate constants (133 K) for hydrated ammonium ions with 19−21 water molecules attached. The dotted line (bottom) indicates average BIRD rate constants for $DiMA^+$ and $TetMA^+$ as a function of cluster size. NH_4^+, $MonMA^+$, nHA^+, tBA^+, and $TriMA^+$ with $n = 20$ have BIRD rate constants that are significantly lower than the average, indicating higher inherent stability, whereas these values for these same ions are significantly higher than the average at $n = 21$, indicating a significant inherent instability.

$TriMA^+{\cdot}(H_2O)_{20}$, for which a MNC was not observed.[58] The appearance of a MNC for this ion may be due to the longer time scale or lower ion temperature of our experiments. Some clusters at other sizes have enhanced abundances as well. For example, $n = 18$ is a MNC for most of the ions, consistent with previous results for ammonium[54,55] and also observed for some alkali metal ions.[48,56,57,64] The enhanced abundance is most pronounced for $tBA^+{\cdot}(H_2O)_{18}$, but $DiMA^+{\cdot}(H_2O)_{18}$ is less abundant than adjacent clusters.

A MNC can occur owing to the inherent stability of an ion with respect to water loss, but it can also be due to the inherent instability of neighboring clusters. To distinguish between these possibilities, BIRD rate constants (133 K) with 19−21 water molecules attached were measured, and the values for each of the ions are shown in Figure 3. BIRD rate constants depend on the rates of radiative absorption and emission as well as the rates of dissociation. In this limited size range, the rates of radiative absorption and emission of the different hydrated ions are expected to be similar. In the absence of specific structural effects, the BIRD rate constants should increase very slightly with increasing cluster size, owing to increasing radiative rates[97] and decreasing threshold dissociation energies for the loss of a water molecule.[98] For $TetMA^+{\cdot}(H_2O)_n$, which has no apparent enhanced abundance at $n = 20$, and for $DiMA^+{\cdot}(H_2O)_n$, for which the abundance of the $n = 20$ cluster is only slightly enhanced, the BIRD rate constants are nearly the same and increase only slightly with increasing cluster size (Figure 3, top). The rate constants for these ions are similar to those measured under the same conditions for the same size nanodrops containing either Li^+ or Na^+, for which cluster abundances in this size range show minimal or no enhancement.[48]

In contrast, the rate constants for NH_4^+, $MonMA^+$, nHA^+, tBA^+, and $TriMA^+$ do not increase monotonically with increasing cluster size (Figure 3, bottom). The clusters with 20 water molecules are significantly more stable than the adjacent size clusters. The average BIRD rate constants for hydrated $DiMA^+$ and $TetMA^+$, for which there are no significant magic numbers in this size range, are plotted as a dashed line in Figure 3, bottom, and this line provides a reference for the expected stability of clusters in the absence of specific structural effects. These data indicate that $Amm{\cdot}(H_2O)_{19}$ clusters, Amm = NH_4^+, $MonMA^+$, nHA^+, tBA^+, and $TriMA^+$, are only slightly less stable than the $DiMA^+$ and $TetMA^+$ containing clusters at this size. In contrast, the former ions are significantly more stable at $n = 20$ and significantly less stable at $n = 21$. These results indicate that the origin of the MNCs at $n = 20$ for NH_4^+, $MonMA^+$, nHA^+, tBA^+, and $TriMA^+$ (Figure 2) is a result of both significant stability of the $n = 20$ clusters and significant instability of the $n = 21$ clusters. The relatively low binding energy of water to the $n = 21$ cluster suggests that addition of a water molecule to the $n = 20$ cluster

dx.doi.org/10.1021/ja407414d | J. Am. Chem. Soc. 2013, 135, 14821−14830

may not significantly change the structure of this cluster, i.e., the core structure that makes the clusters with 20 water molecules especially stable and provides greater stability than what can be gained by optimizing HBs to the additional water molecule in the n = 21 cluster. Although the clusters at n = 19 are less stable than those at n = 20 (Figure 3, bottom), the n = 19 clusters show comparable stability to clusters that do not exhibit magic numbers (Figure 3, top), suggesting that removal of a water molecule from the n = 20 cluster significantly disrupts this core structure.

Spectroscopic Signature for Magic Numbers. IRPD spectra can provide useful insights into structural motifs associated with MNCs. Results from prior IR spectroscopy studies of hydrated H_3O^+,[46,47] NH_4^+,[49] and some alkali metal ions[48] indicate that stable clathrate or cage-like structures are formed at n = 20. The IRPD spectra in the free O−H region (~3640−3780 cm^{-1}) of hydrated ammonium ions with 19−21 water molecules are shown in Figure 4. Bands that appear in this region correspond to stretches of free O−H oscillators, i.e., those that are not hydrogen bonding, and these frequencies are sensitive to the local hydrogen-bonding environment of water molecules at the nanodrop surface.[26,41,46−49,99−103] The spectrum of NH_4^+ with 19 water molecules attached (Figure 4, bottom left) has a band near 3700 cm^{-1} and a shoulder near 3720 cm^{-1}. The 3700 and 3720 cm^{-1} bands correspond to the free O−H stretches of AAD water molecules and water molecules that accept a single HB and donate a single HB (acceptor−donor or AD water molecules), respectively.[26,46−49,100−103] Both of these bands also occur for $NH_4^+\cdot(H_2O)_{21}$. In contrast, the spectrum of $NH_4^+\cdot(H_2O)_{20}$ has only the AAD free O−H feature. These data indicate that there are AD water molecules for clusters at n = 19 and 21 but not at n = 20, consistent with the results of Diken et al. for this ion.[49] IR spectra of the other ions investigated here have not been previously reported. The spectra of MonMA$^+$, nHA$^+$, and tBA$^+$ also have both AD and AAD free O−H bands for n = 19 and 21, but only the AAD free O−H band is present for n = 20.

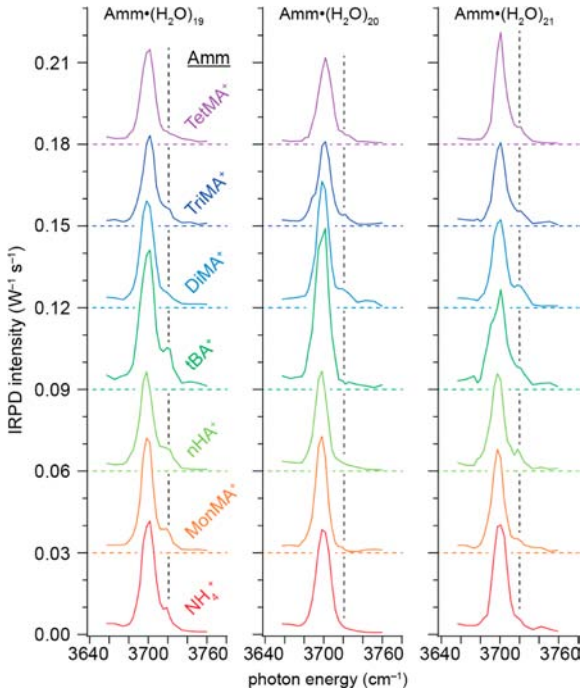

Figure 4. IRPD spectra in the free O−H region for Amm·$(H_2O)_n$ measured at 133 K, where Amm = NH_4^+, MonMA$^+$, nHA$^+$, tBA$^+$, DiMA$^+$, TriMA$^+$, or TetMA$^+$. Horizontal dashed lines indicate a vertical offset of 0.03 W^{-1} s^{-1}.

The spectra of DiMA$^+$, TriMA$^+$, and TetMA$^+$ with n = 19−21 (Figure 4) as well as tBA$^+$ and DiMA$^+$ at n = 18 (Figure S1) each contain both AD and AAD free O−H bands. Thus, these ions do not exhibit the same spectral simplification that occurs for hydrated NH_4^+, MonMA$^+$, nHA$^+$, and tBA$^+$ at n = 20. Although TriMA$^+\cdot(H_2O)_{20}$ and tBA$^+\cdot(H_2O)_{18}$ are MNCs, the small shoulder near 3720 cm^{-1} indicates the presence of AD water molecules, which is not the case for the other MNCs. TriMA$^+$ at n = 20 is the least stable of the MNCs at this size but the most stable at n = 21. Both the presence of AD water molecules and lower relative stability for TriMA$^+\cdot(H_2O)_{20}$ suggest that there may be a mixture of two or more structural families, some of which are less stable.

Integrated Ratios of the AD and AAD Bands. In order to more readily compare the free O−H spectra of these clusters, the ratios of integrated intensities for the AD and AAD features at each hydration state were determined by fitting the spectral bands to two Gaussian peaks centered near 3720 and 3700 cm^{-1}, respectively, and these values are shown in Figure 5.

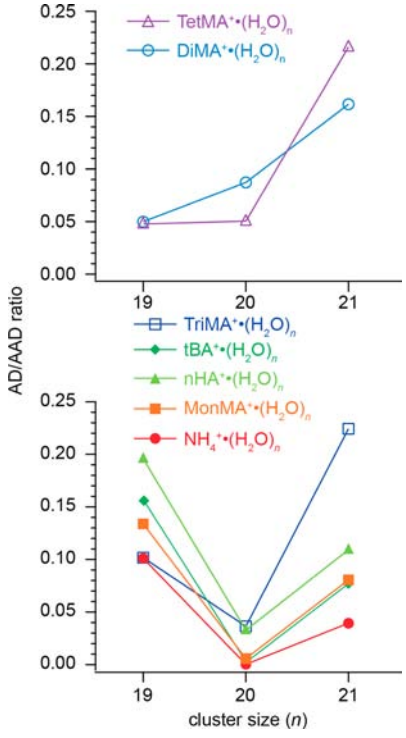

Figure 5. AD/AAD ratio of integrated areas plotted as a function of hydration state. Integrated areas of the AD and AAD bands were calculated from Gaussians centered near 3720 and 3700 cm^{-1}, respectively, that were fitted to the IRPD spectra of each ion in the free O−H region (Figure 4).

The AD/AAD ratios for $NH_4^+\cdot(H_2O)_{20}$, MonMA$^+\cdot(H_2O)_{20}$, and tBA$^+\cdot(H_2O)_{20}$ are <0.01, indicating that there is no measurable contribution from an AD free O−H stretch to these spectra. The AD/AAD ratios for M$^+\cdot(H_2O)_{20}$ (M = K, Rb, and Cs), also MNCs, are ≤0.01.[48] There is no apparent shoulder near 3720 cm^{-1} in the spectrum of nHA$^+\cdot(H_2O)_{20}$, but the integrated ratio is 0.03, which is substantially larger than that of NH_4^+, MonMA$^+$, and tBA$^+$. The higher ratio for nHA$^+\cdot(H_2O)_{20}$

dx.doi.org/10.1021/ja407414d | J. Am. Chem. Soc. 2013, 135, 14821−14830

can be attributed to the asymmetric peak shape of the AAD free O−H band, which may be due to contributions from a minor population of structures containing AD water molecules. In contrast, the AD/AAD ratios for the spectra of NH_4^+, MonMA$^+$, nHA$^+$, and tBA$^+$ with n = 19 or 21 are ≥0.04. These data also show a minimum in the AD/AAD ratio at n = 20 for all of these ions, indicating that the stability of the MNC is related to the absence (or minimization) of the number of AD water molecules.

Interestingly, although the spectra of TriMA$^+\cdot(H_2O)_n$ each contain both the AD and AAD free O−H features, the AD/AAD ratios also exhibit a local minimum at n = 20, suggesting that the relative number of AD water molecules is significantly lower at n = 20 than at n = 19 or 21. In contrast, the AD/AAD ratios for DiMA$^+$ and TetMA$^+$ increase monotonically with increasing hydration state. These data indicate that the minimum in the AD/AAD ratio of TriMA$^+\cdot(H_2O)_{20}$ is associated with its enhanced abundance in the mass spectrum. In addition, both spectra of tBA$^+$ and DiMA$^+$ with 18 water molecules attached have the AD and AAD free O−H bands, but the AD/AAD ratio for tBA$^+\cdot(H_2O)_{18}$ is significantly lower than that of DiMA$^+\cdot(H_2O)_{18}$. This indicates that there is more extensive hydrogen bonding for tBA$^+\cdot(H_2O)_{18}$ than DiMA$^+\cdot(H_2O)_{18}$, consistent with a lower BIRD rate constant for the former ion and its appearance as a MNC in the mass spectrum.

Dodecahedral Clathrate Structures. Previous computational studies of $NH_4^+\cdot(H_2O)_{20}$ indicate that it is favorable for the cluster to form a dodecahedral clathrate structure for which the ion can reside either at the surface or in the interior of the clathrate,[49,76−78] and representative structures are shown in Figure 6a,b, respectively. These clathrate structures have only

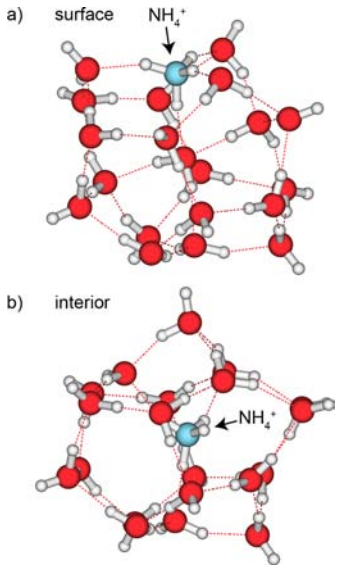

Figure 6. Representative structures for $NH_4^+\cdot(H_2O)_{20}$ with the ion located at the (a) surface or (b) interior of a dodecahedral clathrate structure calculated at the B3LYP/6-31+G** level of theory. Initial geometries were modified from those computed for $H_3O^+\cdot(H_2O)_{20}$.[47]

three and four coordinate water molecules at the surface of nanodrop. Thus, clusters that adopt a dodecahedral structure should only have an AAD band in the free O−H region. The presence of only the AAD band in the spectra of NH_4^+, MonMA$^+$, nHA$^+$, and tBA$^+$ at n = 20 is consistent with a clathrate hydration structure, but both dodecahedral and nondodecahedral clathrate structures have just the AAD band.

Although the IR spectra in the free O−H region provide information about whether a cluster adopts a clathrate structure, the location of ion in the clathrate is more difficult to determine. For NH_4^+, the AD band is predicted to be absent regardless of whether NH_4^+ is located at the surface or the interior.[49] Diken et al. concluded that the location of the ion could not be determined from the IR spectrum of $NH_4^+\cdot(H_2O)_{20}$ alone, but a structure with NH_4^+ at the surface was calculated to be lowest in energy.[49]

Full IRPD Spectra of Hydrated Ammonium Ions. The hydrogen bonded (HB) O−H region (~2600−3650 cm^{-1}) of the spectrum can provide additional information about the structures of these clusters. The full IRPD spectrum, including the free O−H region, of each ammonium ion with 20 water molecules is shown in Figure 7. The spectra generally appear

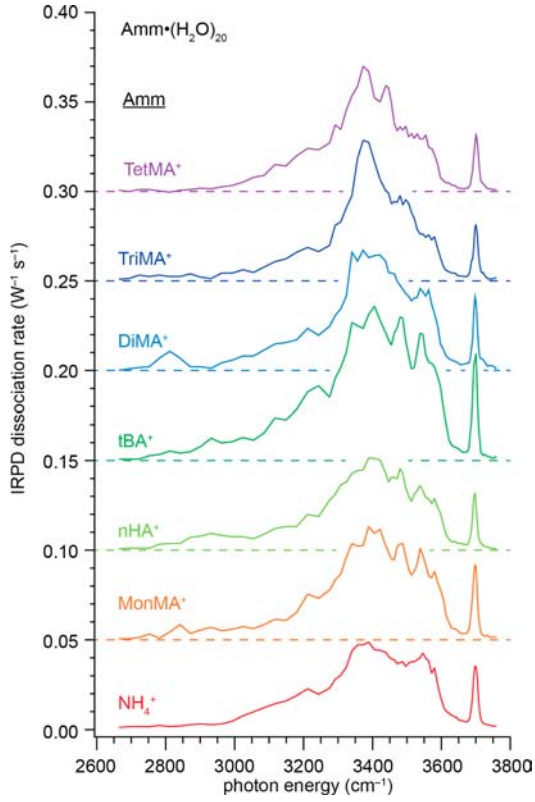

Figure 7. IRPD spectra of Amm$\cdot(H_2O)_{20}$ in both the HB and free O−H regions measured at 133 K, where Amm = NH_4^+, MonMA$^+$, nHA$^+$, tBA$^+$, DiMA$^+$, TriMA$^+$, or TetMA$^+$. Horizontal dashed lines indicate a vertical offset of 0.05 W^{-1} s^{-1}.

quite similar, each containing a relatively sharp band near 3700 cm^{-1} corresponding to the AAD free O−H stretch as well as a broad series of unresolved bands below 3650 cm^{-1} corresponding to HB O−H stretches. Analysis of an individual spectrum is complicated by spectral congestion, but a comparison of the spectra of all the ammonium ions at n = 20 reveals subtle differences. Specifically, each spectrum has two dominant features near 3400 and 3550 cm^{-1} that are similar to those observed for M$^+\cdot(H_2O)_{20}$, where M = Li, Na, K, Rb, and Cs.[48] The band near 3400 cm^{-1} can be assigned to coupled HB O−H stretches,[46−49,102−104] whereas the feature near 3550 cm^{-1} corresponds to the HB O−H stretches of an acceptor−

dx.doi.org/10.1021/ja407414d | J. Am. Chem. Soc. 2013, 135, 14821−14830

donor−donor (ADD) water molecule.[46−48] The relative intensities of the these features depend on the identity of the ion. Information about whether an ion is at the surface or in the interior of the cluster can be obtained by comparing these spectra to reference spectra of ions for which the locations of the ion can be confidently assigned.

Structures of Reference Clusters. The use of reference spectra can aid the analysis of complex spectra of hydrated ions.[40,42,105,106] Recent IRPD results from Cooper et al. as well as computations indicate that K^+, Rb^+, and Cs^+ are located in the interior of clathrates when hydrated by 20 water molecules.[48,64−67] Rb^+ has the same ionic radius as NH_4^+ (1.48 Å),[107] making it a good reference for an ion located at the interior of a clathrate. tBA^+ is very likely to be at the surface of a clathrate owing to the hydrophobic *tert*-butyl group, which disrupts the water hydrogen-bonding network if the ion is in the center. Calculations at the B3LYP/6-31+G** level of theory indicate that structures with tBA^+ in the interior of a clathrate are 86 kJ mol^{-1} or more higher in relative Gibbs free energy (133 K) compared to a structure where the ion is located at the surface (Figure 8). Nonclathrate structures with

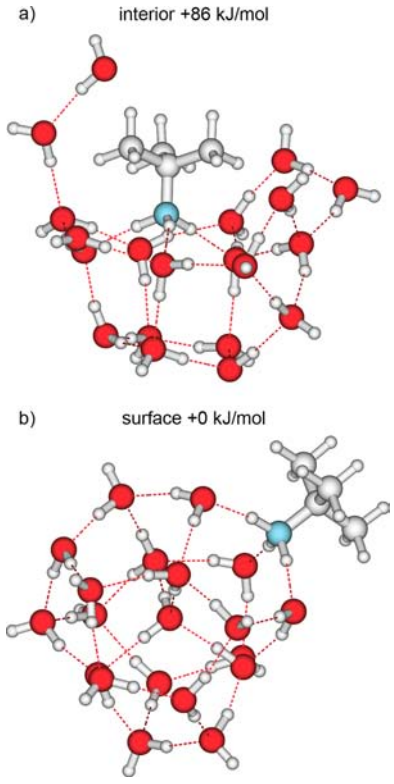

Figure 8. Structures for $tBA^+\cdot(H_2O)_{20}$ with tBA^+ at the (a) interior and at the (b) surface of the droplet. Relative Gibbs free energies (133 K) calculated at the B3LYP/6-31+G** level of theory.

tBA^+ at the surface are calculated to be 18−35 kJ mol^{-1} higher in energy than a dodecahedral clathrate structure with the ion also at the surface. These results indicate $tBA^+\cdot(H_2O)_{20}$ should be a good reference for an ammonium ion located at the surface of a clathrate.

Location of Protonated Primary Amines in a Clathrate Structure. In order to determine how an alkyl group might disrupt the hydrogen-bonding network of a water nanodrop, the locations of $MonMA^+$ and nHA^+ when hydrated by 20 water molecules were determined using the reference spectra. The spectrum of $MonMA^+$ is compared to both reference spectra in Figure 9a. The reference spectra are intensity normalized to one, and the spectrum of $MonMA^+$ is scaled to minimize the residuals (Figure 9a, bottom). The spectra of $MonMA^+$ and tBA^+ with 20 water molecules are nearly the same. In contrast, $MonMA^+$ is a poor match to Rb^+. Compared to Rb^+, the spectrum of $MonMA^+\cdot(H_2O)_{20}$ has an extra band near 3450 cm^{-1}, there is a small shift in the band at 3400 cm^{-1}, and the two bands near 3550 cm^{-1} have slightly different shapes.

The quality of a match between two spectra is reflected by the root-mean-square (RMS) value of the residuals (Table 1). These data indicate that the spectrum of $MonMA^+\cdot(H_2O)_{20}$ is more similar to $tBA^+\cdot(H_2O)_{20}$ (RMS = 0.04) than to $Rb^+\cdot(H_2O)_{20}$ (RMS = 0.08). By comparison, two spectra of $NH_4^+\cdot(H_2O)_{20}$ measured on different days had a RMS = 0.04, indicating the limit of reproducibility in these experiments. Even though tBA^+ has three methyl groups compared to one for $MonMA^+$, the spectra are essentially indistinguishable. C−H stretches appear between 2950 and 3150 cm^{-1}, yet there is little difference in intensity in this region, consistent with prior observations that these are typically weak bands in IRPD spectra.[41,43,105,108] The close match between $MonMA^+\cdot(H_2O)_{20}$ and $tBA^+\cdot(H_2O)_{20}$ suggests that they adopt similar structures in which $MonMA^+$ is located at the surface of a clathrate. Similarly, the RMS values obtained for nHA^+ (Table 1) indicate that nHA^+ closely matches tBA^+ (RMS = 0.04) and is a poor match to Rb^+ (RMS = 0.10). This indicates that nHA^+ is also located at the clathrate surface. If nHA^+ is used instead of tBA^+ as the reference for an ion at the surface, the RMS from a comparison to $MonMA^+$ is also 0.04. Thus, the same result is obtained whether tBA^+ or nHA^+ is used as the reference for an ion at the surface. These comparisons suggest that protonated primary amines are at the surface of a clathrate irrespective of the length or size of the alkyl group attached to the nitrogen atom.

Location of Ammonium in a Clathrate Structure. In contrast to $MonMA^+$ and nHA^+ at n = 20, the spectrum of $NH_4^+\cdot(H_2O)_{20}$ is nearly identical to that of $Rb^+\cdot(H_2O)_{20}$ (Figure 9b). Both spectra have similar bands near 3400 and 3550 cm^{-1}, and neither has a significant band at ∼3450 cm^{-1} observed for primary amines and for tBA^+. The RMS value between NH_4^+ and Rb^+ is 0.05, but this relatively high value can be attributed to a fundamental difference between these two ions. The residuals near 3100 cm^{-1} are consistent with HB N−H stretches[102] for $NH_4^+\cdot(H_2O)_{20}$, which are absent for $Rb^+\cdot(H_2O)_{20}$. The residuals near 3700 cm^{-1} are due to a shift in the free O−H band, which can be attributed to NH_4^+ forming HBs to water molecules, whereas Rb^+ cannot. These HBs can cause slight differences in the hydrogen-bonding environment of the AAD water molecules resulting in the small shift in the free O−H frequency. The spectra of $NH_4^+\cdot(H_2O)_{20}$ and $Rb^+\cdot(H_2O)_{20}$ closely match, whereas the spectra of $NH_4^+\cdot(H_2O)_{20}$ and $tBA^+\cdot(H_2O)_{20}$ do not match nearly as well (RMS = 0.07). There is poor overlap between the bands at ∼3400 and ∼3550 cm^{-1}, and the spectrum of $tBA^+\cdot(H_2O)_{20}$ has the extra band near 3450 cm^{-1}. A comparison between nHA^+ and NH_4^+ also yields the same RMS value (0.07) as between tBA^+ and NH_4^+. These results show that $NH_4^+\cdot(H_2O)_{20}$ adopts a similar structure to that of $Rb^+\cdot(H_2O)_{20}$, indicating that NH_4^+ is located in the interior of a clathrate.

Reference Comparisons to Other Alkylammonium Ions. Similar comparisons were performed for $DiMA^+$,

dx.doi.org/10.1021/ja407414d | J. Am. Chem. Soc. 2013, 135, 14821−14830

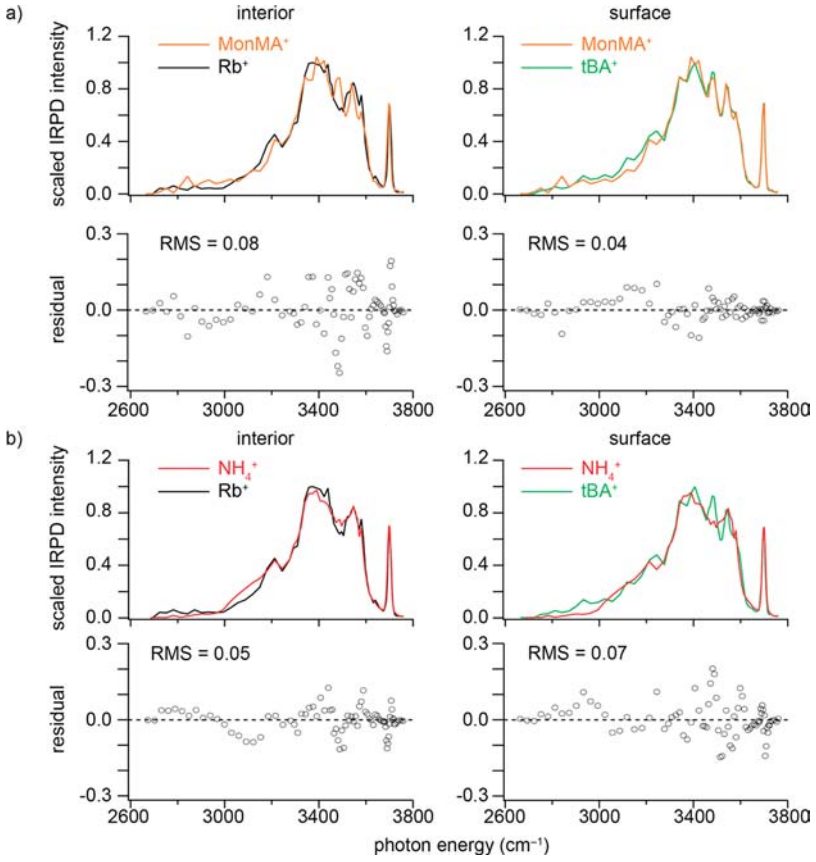

Figure 9. Comparisons of the IRPD spectra of (a) $MonMA^+\cdot(H_2O)_{20}$ and (b) $NH_4^+\cdot(H_2O)_{20}$ with $Rb^+\cdot(H_2O)_{20}$, which is a reference of a clathrate structure with the ion in the interior, and $tBA^+\cdot(H_2O)_{20}$, which is a reference for a clathrate structure with the ion at the surface. The RMS of the residuals are below. The high similarity between the IRPD spectra of $MonMA^+\cdot(H_2O)_{20}$ and $tBA^+(H_2O)_{20}$ indicates that $MonMA^+$ is at the surface of a clathrate structure. In contrast, the similarity between the IRPD spectra of $NH_4^+\cdot(H_2O)_{20}$ and $Rb^+\cdot(H_2O)_{20}$ indicates that ammonium is located in the center of a clathrate structure.

Table 1. Calculated RMS of Residuals for Comparisons with Reference Spectra

	interior	surface
	(Rb^+)	(tBA^+)
NH_4^+	0.05	0.07
$MonMA^+$	0.08	0.04
nHA^+	0.10	0.04
$DiMA^+$	0.08	0.08
$TriMA^+$	0.14	0.14
$TetMA^+$	0.13	0.15

$TriMA^+$, and $TetMA^+$ with n = 20. The RMS values obtained from these comparisons (Table 1) are ≥0.08, indicating that $DiMA^+$, $TriMA^+$, and $TetMA^+$ are poor matches to either reference ion. The poor matches can be attributed to the presence of nonclathrate structures. The free O−H spectra of $DiMA^+$, $TriMA^+$, and $TetMA^+$ for n = 20 have an AD free O−H band, indicating that a significant fraction of the ion population adopts nonclathrate structures. In contrast, the absence of this band for of Rb^+ and tBA^+ with 20 water molecules suggests that these ions form clathrate structures nearly exclusively. Because $DiMA^+$, $TriMA^+$ and $TetMA^+$ adopt nonclathrate structures when hydrated by 20 water molecules, Rb^+ and tBA^+ are unsuitable reference ions.

Relative Energies of Clathrate vs Nonclathrate Structures. The origin of nonclathrate structures present for $DiMA^+$, $TriMA^+$ and $TetMA^+$ at n = 20 was investigated with computational chemistry to determine the relative energy differences between clathrate and nonclathrate structures. The relative energies and the number of water−water HBs of low-energy structures calculated for $DiMA^+$, $TriMA^+$ and $TetMA^+$ are shown in Figure 10 and are summarized in Table 2. For all three ions, a dodecahedral clathrate structure (Figure S2) was found to be lowest in energy, and this structure has the highest number of HBs. The difference in Gibbs free energy (133 K) between a clathrate and nonclathrate structure for $TriMA^+$ is calculated to be 18 kJ mol^{-1}. In contrast, the relative energy differences for $DiMA^+$ and $TetMA^+$ are significantly lower (13 and 3 kJ mol^{-1}, respectively). The lower differences in relative Gibbs free energies for $DiMA^+\cdot(H_2O)_{20}$ and $TetMA^+\cdot(H_2O)_{20}$ in comparison to that for $TriMA^+\cdot(H_2O)_{20}$ are consistent with the trends in relative intensities of the AD free O−H band observed for these ions. There is a noticeable shoulder corresponding to the AD free O−H for $DiMA^+\cdot(H_2O)_{20}$ and $TetMA^+\cdot(H_2O)_{20}$, whereas this is only a minor feature for $TriMA^+\cdot(H_2O)_{20}$. Although dodecahedral structures maximize the number of HBs, structures with fewer HBs were found to energetically competitive. In addition, there does not appear to be a direct correlation between the relative energy of a structure and the number of HBs. These results indicate the relative stabilities of clathrate structures are not solely a result of maximizing the number of HBs. Other factors, such as the

dx.doi.org/10.1021/ja407414d | J. Am. Chem. Soc. 2013, 135, 14821−14830

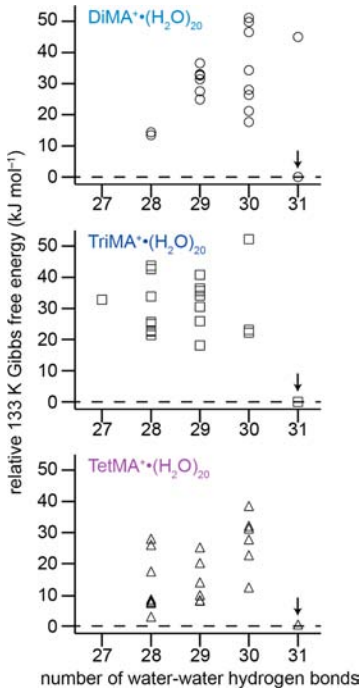

Figure 10. Relative 133 K Gibbs free energies (kJ mol^{-1}) of low-energy structures for Amm·$(H_2O)_{20}$ (Amm = $DiMA^+$, $TriMA^+$, and $TetMA^+$) calculated at the B3LYP/6-31+G** level of theory plotted as a function of the number of water−water hydrogen bonds in the cluster. The lowest-energy dodecahedral clathrate structures are indicated with an arrow.

Table 2. Range and Mean (in parentheses) of Relative Gibbs Free Energies (133 K) in kJ mol^{-1} for Calculated Structures (B3LYP/6-31+G level of theory) with a Given Number of Water−Water Hydrogen Bonds (WW HBs) within the Cluster**

WW HBs	$DiMA^+·(H_2O)_{20}$	$TriMA^+·(H_2O)_{20}$	$TetMA^+·(H_2O)_{20}$
27	–	33	–
28	13−14 (13.8)	21−44 (28.8)	3−28 (12.8)
29	25−37 (30.8)	18−41 (31.6)	8−25 (13.8)
30	18−51 (34.4)	22−52 (32.5)	12−25 (27.0)
31	0−45 (22.5)	0	0

orientation and thus the strength of HBs in the water network, contribute to the overall stabilities of clathrate structures.

CONCLUSION

IRPD spectroscopy in the region between 2600 and 3800 cm^{-1} was used to distinguish whether protonated primary amines and ammonia are located at the surface or in the interior of a clathrate consisting of 20 water molecules. For these ions, clathrate structures are indicated by the characteristic AAD free O−H stretch and the absence of an AD free O−H stretch. However, the location of these ions cannot be determined from these data alone. A comparison of IRPD spectra that includes HB O−H stretches shows subtle but important differences. The location of the ion at the surface or in the interior of the nanodrop is elucidated by comparisons to IRPD spectra of reference ions for which the location of the ion can be confidently assigned. Rb^+ is used as a reference for an ion at the interior of the clathrate[48] due to its similar ionic radius as NH_4^+,[107] and protonated *tert*-butylamine is used as a reference for an ion at the surface of the nanodrop. IRPD spectra indicate that the latter ion is a clathrate, and structures with the ion in the interior are calculated to be 86 kJ mol^{-1} higher in energy than those with the ion at the surface. Results from these comparisons indicate that protonated ammonia is located in the interior of the clathrate, whereas protonated methylamine and protonated *n*-heptylamine are at the surface. Results for protonated secondary and tertiary amines as well as $TetMA^+$ were ambiguous because structures other than clathrates are competitive for these ions making Rb^+ and tBA^+ unsuitable as references.

The interior location of NH_4^+ and Rb^+ in a clathrate structure with 20 water molecules compared to the surface location for $MonMA^+$, nHA^+ and tBA^+ is likely a result of the propensity of the latter ions to adversely affect the hydrogen-bonding network of the very stable clathrate structure when these ions are located in the interior. There is no direct correlation between stability and the number of HBs in a structure, indicating that the orientation of the hydrogen-bonding network as well as the overall number of HBs are critical to stability. These are the first experimental results showing that NH_4^+ is in the interior of a clathrate structure with 20 water molecules, and these results should provide a benchmark for future computational studies aimed at determining the propensity for ions to be surface active.

ASSOCIATED CONTENT

Supporting Information

Full citation for ref 96 and calculated clathrate structures for selected ions can be found. This information is available free of charge via the Internet at http://pubs.acs.org.

AUTHOR INFORMATION

Corresponding Author

erw@berkeley.edu

Notes

The authors declare no competing financial interest.

ACKNOWLEDGMENTS

The authors wish to thank the National Science Foundation (grant CHE-1012833 and CHE-1306720) for generous financial support of this research and for the support of the University of California, Berkeley Molecular Graphics and Computation Facility (CHE-0840505).

REFERENCES

(1) Schreier, S.; Malheiros, S. V. P.; de Paula, E. *Biochim. Biophys. Acta* **2000**, *1508*, 210−234.
(2) Jin, Y. G.; Chen, S. F.; Xin, R.; Zhou, Y. S. *Colloids Surf., B* **2008**, *64*, 229−235.
(3) Kabir-ud-Din; Khan, A. B.; Naqvi, A. Z. *Phys. Chem. Liq.* **2012**, *50*, 478−494.
(4) Tsai, C. J.; Nussinov, R. *Protein Sci.* **1997**, *6*, 1426−1437.
(5) Vanhee, P.; Stricher, F.; Baeten, L.; Verschueren, E.; Lenaerts, T.; Serrano, L.; Rousseau, F.; Schymkowitz, J. *Structure* **2009**, *17*, 1128−1136.
(6) Krishnaswamy, S. R.; Williams, E. R.; Kirsch, J. F. *Protein Sci.* **2006**, *15*, 1465−1475.
(7) Percy, A. J.; Rey, M.; Burns, K. M.; Schriemer, D. C. *Anal. Chim. Acta* **2012**, *721*, 7−21.
(8) Hunt, S. W.; Roeselova, M.; Wang, W.; Wingen, L. M.; Knipping, E. M.; Tobias, D. J.; Dabdub, D.; Finlayson-Pitts, B. J. *J. Phys. Chem. A* **2004**, *108*, 11559−11572.

(9) Nissenson, P.; Packwood, D. M.; Hunt, S. W.; Finlayson-Pitts, B. J.; Dabdub, D. *Atmos. Environ.* **2009**, *43*, 3951−3962.
(10) Richards, N. K.; Wingen, L. M.; Callahan, K. M.; Nishino, N.; Kleinman, M. T.; Tobias, D. J.; Finlayson-Pitts, B. J. *J. Phys. Chem. A* **2011**, *115*, 5810−5821.
(11) Jubb, A. M.; Hua, W.; Allen, H. C. *Annu. Rev. Phys. Chem.* **2012**, *63*, 107−130.
(12) Li, R. H.; Jiang, Z. P.; Chen, F. G.; Yang, H. W.; Guan, Y. T. *J. Mol. Struct.* **2004**, *707*, 83−88.
(13) Guardia, E.; Laria, D.; Marti, J. *J. Phys. Chem. B* **2006**, *110*, 6332−6338.
(14) Miller, D. J.; Lisy, J. M. *J. Am. Chem. Soc.* **2008**, *130*, 15393−15404.
(15) O'Brien, J. T.; Prell, J. S.; Bush, M. F.; Williams, E. R. *J. Am. Chem. Soc.* **2010**, *132*, 8248−8249.
(16) O'Brien, J. T.; Williams, E. R. *J. Am. Chem. Soc.* **2012**, *134*, 10228−10236.
(17) Prell, J. S.; O'Brien, J. T.; Williams, E. R. *J. Am. Chem. Soc.* **2011**, *133*, 4810−4818.
(18) Marcus, Y. *Pure Appl. Chem.* **2010**, *82*, 1889−1899.
(19) Hofmeister, F. *Arch. Exp. Pathol. Pharmacol.* **1888**, *24*, 247−260.
(20) Baldwin, R. L. *Biophys. J.* **1996**, *71*, 2056−2063.
(21) Rembert, K. B.; Paterova, J.; Heyda, J.; Hilty, C.; Jungwirth, P.; Cremer, P. S. *J. Am. Chem. Soc.* **2012**, *134*, 10039−10046.
(22) Stuart, S. J.; Berne, B. J. *J. Phys. Chem. A* **1999**, *103*, 10300−10307.
(23) Jungwirth, P.; Tobias, D. J. *Chem. Rev.* **2006**, *106*, 1259−1281.
(24) Ishiyama, T.; Morita, A. *J. Phys. Chem. C* **2007**, *111*, 721−737.
(25) Hagberg, D.; Brdarski, S.; Karlstrom, G. *J. Phys. Chem. B* **2005**, *109*, 4111−4117.
(26) Walters, R. S.; Pillai, E. D.; Duncan, M. A. *J. Am. Chem. Soc.* **2005**, *127*, 16599−16610.
(27) O'Brien, J. T.; Williams, E. R. *J. Phys. Chem. A* **2011**, *115*, 14612−14619.
(28) Cooper, T. E.; O'Brien, J. T.; Williams, E. R.; Armentrout, P. B. *J. Phys. Chem. A* **2010**, *114*, 12646−12655.
(29) Misaizu, F.; Sanekata, M.; Fuke, K.; Iwata, S. *J. Chem. Phys.* **1994**, *100*, 1161−1170.
(30) Robertson, W. H.; Diken, E. G.; Price, E. A.; Shin, J. W.; Johnson, M. A. *Science* **2003**, *299*, 1367−1372.
(31) Gao, B.; Wyttenbach, T.; Bowers, M. T. *J. Am. Chem. Soc.* **2009**, *131*, 4695−4701.
(32) Lemoff, A. S.; Bush, M. F.; Wu, C. C.; Williams, E. R. *J. Am. Chem. Soc.* **2005**, *127*, 10276−10286.
(33) Gao, B.; Wyttenbach, T.; Bowers, M. T. *J. Phys. Chem. B* **2009**, *113*, 9995−10000.
(34) Lemoff, A. S.; Williams, E. R. *J. Am. Mass. Spectrom.* **2004**, *15*, 1014−1024.
(35) Klassen, J. S.; Blades, A. T.; Kebarle, P. *J. Phys. Chem.* **1995**, *99*, 15509−15517.
(36) Meot-Ner, M.; Field, F. H. *J. Am. Chem. Soc.* **1974**, *96*, 3168−3171.
(37) Wincel, H. *J. Phys. Chem. A* **2007**, *111*, 5784−5791.
(38) Ye, S. J.; Moision, R. M.; Armentrout, P. B. *Int. J. Mass Spectrom.* **2006**, *253*, 288−304.
(39) Carl, D. R.; Armentrout, P. B. *ChemPhysChem* **2013**, *14*, 681−697.
(40) Bush, M. F.; Prell, J. S.; Saykally, R. J.; Williams, E. R. *J. Am. Chem. Soc.* **2007**, *129*, 13544−13553.
(41) Kamariotis, A.; Boyarkin, O. V.; Mercier, S. R.; Beck, R. D.; Bush, M. F.; Williams, E. R.; Rizzo, T. R. *J. Am. Chem. Soc.* **2006**, *128*, 905−916.
(42) Chang, T. M.; Prell, J. S.; Warrick, E. R.; Williams, E. R. *J. Am. Chem. Soc.* **2012**, *134*, 15805−15813.
(43) Demireva, M.; O'Brien, J. T.; Williams, E. R. *J. Am. Chem. Soc.* **2012**, *134*, 11216−11224.
(44) Wende, T.; Wanko, M.; Jiang, L.; Meijer, G.; Asmis, K. R.; Rubio, A. *Angew. Chem., Int. Ed.* **2011**, *50*, 3807−3810.
(45) Ayotte, P.; Bailey, C. G.; Weddle, G. H.; Johnson, M. A. *J. Phys. Chem. A* **1998**, *102*, 3067−3071.
(46) Miyazaki, M.; Fujii, A.; Ebata, T.; Mikami, N. *Science* **2004**, *304*, 1134−1137.
(47) Shin, J.-W.; Hammer, N. I.; Diken, E. G.; Johnson, M. A.; Walters, R. S.; Jaeger, T. D.; Duncan, M. A.; Christie, R. A.; Jordan, K. D. *Science* **2004**, *304*, 1137−1140.
(48) Cooper, R. J.; Chang, T. M.; Williams, E. R. *J. Phys. Chem. A* **2013**, *117*, 6571−6579.
(49) Diken, E. G.; Hammer, N. I.; Johnson, M. A.; Christie, R. A.; Jordan, K. D. *J. Chem. Phys.* **2005**, *123*, 164309.
(50) Lin, S. S. *Rev. Sci. Instrum.* **1973**, *44*, 516−517.
(51) Searcy, J. Q.; Fenn, J. B. *J. Chem. Phys.* **1974**, *61*, 5282−5288.
(52) Wu, C. C.; Lin, C. K.; Chang, H. C.; Jiang, J. C.; Kuo, J. L.; Klein, M. L. *J. Chem. Phys.* **2005**, *122*, 074315.
(53) Shinohara, H.; Nagashima, U.; Tanaka, H.; Nishi, N. *J. Chem. Phys.* **1985**, *83*, 4183−4192.
(54) Schmidt, M.; Masson, A.; Brechignac, C.; Cheng, H. P. *J. Chem. Phys.* **2007**, *126*, 154315.
(55) Ryding, M. J.; Ruusuvuori, K.; Andersson, P. U.; Zatula, A. S.; McGrath, M. J.; Kurten, T.; Ortega, I. K.; Vehkamaki, H.; Uggerud, E. *J. Phys. Chem. A* **2012**, *116*, 4902−4908.
(56) Selinger, A.; Castleman, A. W. *J. Phys. Chem.* **1991**, *95*, 8442−8444.
(57) Lee, S. W.; Freivogel, P.; Schindler, T.; Beauchamp, J. L. *J. Am. Chem. Soc.* **1998**, *120*, 11758−11765.
(58) Nguyen, V. Q.; Chen, X. G.; Yergey, A. L. *J. Am. Soc. Mass Spectrom.* **1997**, *8*, 1175−1179.
(59) Nagashima, U.; Shinohara, H.; Nishi, N.; Tanaka, H. *J. Chem. Phys.* **1986**, *84*, 209−214.
(60) Kassner, J. L.; Hagen, D. E. *J. Chem. Phys.* **1976**, *64*, 1860−1861.
(61) Holland, P. M.; Castleman, A. W. *J. Chem. Phys.* **1980**, *72*, 5984.
(62) Hermann, V.; Kay, B. D.; Castleman, A. W. *Chem. Phys.* **1982**, *72*, 185−200.
(63) Silveira, J. A.; Servage, K. A.; Gamage, C. M.; Russell, D. H. *J. Phys. Chem. A* **2013**, *117*, 953−961.
(64) Steel, E. A.; Merz, K. M.; Selinger, A.; Castleman, A. W. *J. Phys. Chem.* **1995**, *99*, 7829−7836.
(65) Khan, A. *Chem. Phys. Lett.* **2004**, *388*, 342−347.
(66) Schulz, F.; Hartke, B. *ChemPhysChem* **2002**, *3*, 98−106.
(67) Schulz, F.; Hartke, B. *Theor. Chem. Acc.* **2005**, *114*, 357−379.
(68) Buffey, I. P.; Brown, W. B. *Chem. Phys. Lett.* **1984**, *109*, 59−65.
(69) Kozack, R. E.; Jordan, P. C. *J. Chem. Phys.* **1993**, *99*, 2978−2984.
(70) Khan, A. *Chem. Phys. Lett.* **1994**, *217*, 443−450.
(71) Khan, A. 2000, *319*, 440-450.
(72) Hodges, M. P.; Wales, D. J. *Chem. Phys. Lett.* **2000**, *324*, 279−288.
(73) Iyengar, S. S.; Petersen, M. K.; Day, T. J. F.; Burnham, C. J.; Teige, V. E.; Voth, G. A. *J. Chem. Phys.* **2005**, *123*, 084309.
(74) Singh, N. J.; Park, M.; Min, S. K.; Suh, S. B.; Kim, K. S. *Angew. Chem., Int. Ed.* **2006**, *45*, 3795−3800.
(75) Kus, T.; Lotrich, V. F.; Perera, A.; Bartlett, R. J. *J. Chem. Phys.* **2009**, *131*, 104313.
(76) Khan, A. *Chem. Phys. Lett.* **2001**, *338*, 201−207.
(77) Douady, J.; Calvo, F.; Spiegelman, F. *J. Chem. Phys.* **2008**, *129*, 154305.
(78) Willow, S. Y.; Singh, N. J.; Kim, K. S. *J. Chem. Theory Comput.* **2011**, *7*, 3461−3465.
(79) Wei, S.; Shi, Z.; Castleman, A. W. *J. Chem. Phys.* **1991**, *94*, 3268−3270.
(80) Kennett, J. P.; Cannariato, K. G.; Hendy, I. L.; Behl, R. J. *Science* **2000**, *288*, 128−133.
(81) Koh, C. A.; Sloan, E. D.; Sum, A. K.; Wu, D. T. *Annu. Rev. Chem. Biomol. Eng.* **2011**, *2*, 237−257.
(82) Seo, Y.; Kang, S. P. *Chem. Eng. J.* **2010**, *161*, 308−312.
(83) Zhang, B. Y.; Wu, Q. *Energy Fuels* **2010**, *24*, 2530−2535.
(84) Eslamimanesh, A.; Mohammadi, A. H.; Richon, D.; Naidoo, P.; Ramjugernath, D. *J. Chem. Thermodyn.* **2012**, *46*, 62−71.

(85) Booth, J. S.; Rowe, M. M.; Fischer, K. M. Open File Report 1 for U.S. Geological Survey: Reston, VA, 1996, pp 96−272.
(86) Collett, T. S. *AAPG Bull.* **2002**, *86*, 1971−1992.
(87) Milkov, A. V. *Earth Sci. Rev.* **2004**, *66*, 183−197.
(88) Gonzalez, B. S.; Hernandez-Rojas, J.; Wales, D. J. *Chem. Phys. Lett.* **2005**, *412*, 23−28.
(89) Agmon, N. *Chem. Phys. Lett.* **1995**, *244*, 456−462.
(90) Tuckerman, M.; Laasonen, K.; Sprik, M.; Parrinello, M. *J. Phys. Chem.* **1995**, *99*, 5749−5752.
(91) Geissler, P. L.; Dellago, C.; Chandler, D.; Hutter, J.; Parrinello, M. *Science* **2001**, *291*, 2121−2124.
(92) Lockwood, G. K.; Garofalini, S. H. *J. Phys. Chem. B* **2013**, *117*, 4089−4097.
(93) Bush, M. F.; O'Brien, J. T.; Prell, J. S.; Saykally, R. J.; Williams, E. R. *J. Am. Chem. Soc.* **2007**, *129*, 1612−1622.
(94) Wong, R. L.; Paech, K.; Williams, E. R. *Int. J. Mass Spectrom.* **2004**, *232*, 59−66.
(95) Prell, J. S.; O'Brien, J. T.; Williams, E. R. *J. Am. Mass. Spectrom.* **2010**, *21*, 800−809.
(96) Shao, Y.; et al. *Phys. Chem. Chem. Phys.* **2006**, *8*, 3172−3191.
(97) Price, W. D.; Schnier, P. D.; Jockusch, R. A.; Strittmatter, E. F.; Williams, E. R. *J. Am. Chem. Soc.* **1996**, *118*, 10640−10644.
(98) Donald, W. A.; Williams, E. R. *J. Phys. Chem. A* **2008**, *112*, 3515−3522.
(99) Cheng, T. C.; Bandyopadhyay, B.; Mosley, J. D.; Duncan, M. A. *J. Am. Chem. Soc.* **2012**, *134*, 13046−13055.
(100) Chang, H. C.; Wu, C. C.; Kuo, J. L. *Int. Rev. Phys. Chem.* **2005**, *24*, 553−578.
(101) Nicely, A. L.; Miller, D. J.; Lisy, J. M. *J. Mol. Spectrosc.* **2009**, *257*, 157−163.
(102) Chang, H. C.; Wang, Y. S.; Lee, Y. T. *Int. J. Mass Spectrom.* **1998**, *180*, 91−102.
(103) Bush, M. F.; Saykally, R. J.; Williams, E. R. *J. Am. Chem. Soc.* **2008**, *130*, 15482−15489.
(104) Nagornova, N. S.; Rizzo, T. R.; Boyarkin, O. V. *Science.* **2012**, *336*, 320−323.
(105) Prell, J. S.; Chang, T. M.; O'Brien, J. T.; Williams, E. R. *J. Am. Chem. Soc.* **2010**, *132*, 7811−7819.
(106) Prell, J. S.; Correra, T. C.; Chang, T. M.; Biles, J. A.; Williams, E. R. *J. Am. Chem. Soc.* **2010**, *132*, 14733−14735.
(107) Conway, B. E. *Ionic Hydration in Chemistry and Biophysics*; Elsevier: New York, 1981.
(108) Atkins, C. G.; Rajabi, K.; Gillis, E. A. L.; Fridgen, T. D. *J. Phys. Chem. A* **2008**, *112*, 10220−10225.